



# New approaches in global ionospheric determination using ground GPS data

M. Hernández-Pajares\*, J.M. Juan, J. Sanz

*Group of Astronomy and Geomatics, Department of Applied Mathematics and Telematics, and Department of Applied Physics, Universitat Politècnica de Catalunya, Jordi Girona 1;3, 08034, Barcelona, Spain*

Received 23 January 1999; received in revised form 24 June 1999; accepted 30 June 1999

## Abstract

Since 1 June 1998, the group of Astronomy and Geomatics of the Polytechnic University of Catalonia (gAGE/UPC) is contributing to the international project of defining an ionospheric product (Total Electron Content, TEC) from the data gathered by the permanent ground GPS receivers of the International GPS Service (IGS) network. The strategy and algorithms related to such a preliminary product, its calibration with synthetic observations generated from the International Reference Ionosphere (IRI), and the comparison with TOPEX TEC data are presented. Finally, these methods are applied combining ionosonde with ground GPS data, in order to obtain the vertical structure of the free electron distribution. © 2000 Elsevier Science Ltd. All rights reserved.

## 1. Introduction

Recently the feasibility of the tomographic approach has been shown in order to estimate the ionospheric electron density at global scale from GPS data, including difficult scenarios with high geomagnetic activity (Hernández-Pajares et al., 1998a). In that work the GPS pseudo-ranges are not considered, and only the more precise L1 and L2 carrier phases are used. The results obtained have suggested to the authors the application of these new approaches to other existing observational scenarios:

1. to improve the Total Electron Content (TEC) estimation at the global scale using only ground data. This is done by means of the implementation of

coarse tomographic models to diminish the electron content mismodelling and the use of carrier phase data uniquely. These techniques are being applied on a daily basis by our group, in the context of the international effort to define a common IGS ionospheric (TEC) product (Feltens and Schaer, 1998). The details of the global strategy used, the validation with the synthetic observations provided by the International Reference Ionosphere (IRI) model (Bilitza, 1990), the comparison with TOPEX TEC data, and an alternative multistation approach are described in this paper;

2. to combine both ground GPS and ionosonde data: in Hernández-Pajares et al. (1998b) the tomographic electron density model can be solved — and successfully compared with ionosonde profiles — due to the combined use of ground and Low Earth Orbiter (LEO) GPS data. In this paper we are going to study the capability of solving for a 4D electron density model using ionosonde data instead of LEO GPS data to obtain information on the vertical structure.

\* Corresponding author. Tel.: +34-93-401-6029; fax: +34-93-401-5981.

E-mail address: manuel@mat.upc.es (M. Hernández-Pajares).

## 2. Model

### 2.1. Preprocess

Two stages can be distinguished in the preprocessing: first the ionospheric combination,  $\mathcal{L}_I \equiv \mathcal{L}_1 - \mathcal{L}_2$ , is formed from the raw carrier phase observations taken in the two frequencies  $f_1 \approx 1.6$  GHz ( $\mathcal{L}_1$ ) and  $f_2 \approx 1.2$  GHz ( $\mathcal{L}_2$ ), and, second, the cycle slips are detected, splitting the data in arcs of continuous phase transmitter-receiver. Then,  $\mathcal{L}_I$  can be modeled for each arc as:

$$\mathcal{L}_I = \kappa \int_{\vec{r}^T(t^T)}^{\vec{r}^R(t^R)} N_e(\vec{r}, t) ds + \lambda_1 b_1 - \lambda_2 b_2 \quad (1)$$

being  $\kappa \approx 1.05$  m of  $\mathcal{L}_I / 10^{17}$  electrons  $m^{-2}$ ,  $N_e(\vec{r}, t)$  the electron density at each point  $\vec{r}$  of the ray-path observed at time  $t$ , where the integral is considered:  $\vec{r}^T$  is the position of transmitter  $T$  at the transmission time  $t^T$ , and  $\vec{r}^R$  the position of receiver  $R$  at the reception time  $t^R$ . The term including ambiguity and instrumental delays,  $\lambda_1 b_1 - \lambda_2 b_2$ , can be considered constant for each single arc (more details can be found in Hernández-Pajares et al. (1998a)).

We assume a stationary electron density  $N_e(\vec{r}, t)$  in a solar fixed reference frame, with time scales of 2 h. In general this is not a strong assumption, taking into account that the ionization is mainly driven by the Sun.

The fundamental data for our approach are the car-

rier phase differences referred to the first point of the transmitter-receiver continuous phase are ( $\Delta \mathcal{L}_I$ ):

$$\frac{\Delta \mathcal{L}_I}{\kappa} = \int_{\vec{r}^T(t^T+\tau)}^{\vec{r}^R(t^R+\tau)} N_e ds - \int_{\vec{r}^T(t^T)}^{\vec{r}^R(t^R)} N_e ds \quad (2)$$

Taking phase differences relative to the first point of the given arc, the geometric variation is maximized providing strength to the inversion problem. Notice that, in this way, we avoid the estimation of the differential code biases, with the unique assumption that they do not change in an arc of continuous carrier phase (typically during less than 4 h).

There are more conventional strategies of estimating the electron content, without using differences but using the code to align the phase (i.e. estimating the corresponding ambiguity) and, in a second step, solving simultaneously the instrumental delays with the electron content (Mannucci et al., 1998). However, these strategies are affected by an error in the alignment process due to the code noise, more important with anti-spoofing status and at low elevation angles (affected by multipath). The code noise can reach several TECU (1 TECU =  $10^{16}$  electrons/ $m^2$ ) depending on the receiver type. Using an elevation mask (typically  $10^\circ$  or higher) the noisier data are excluded. But these rays contain the greatest part of the information about the vertical structure needed to get a better TEC estimation by means of a two-layer tomographic model, as discussed later. In our strategy the carrier

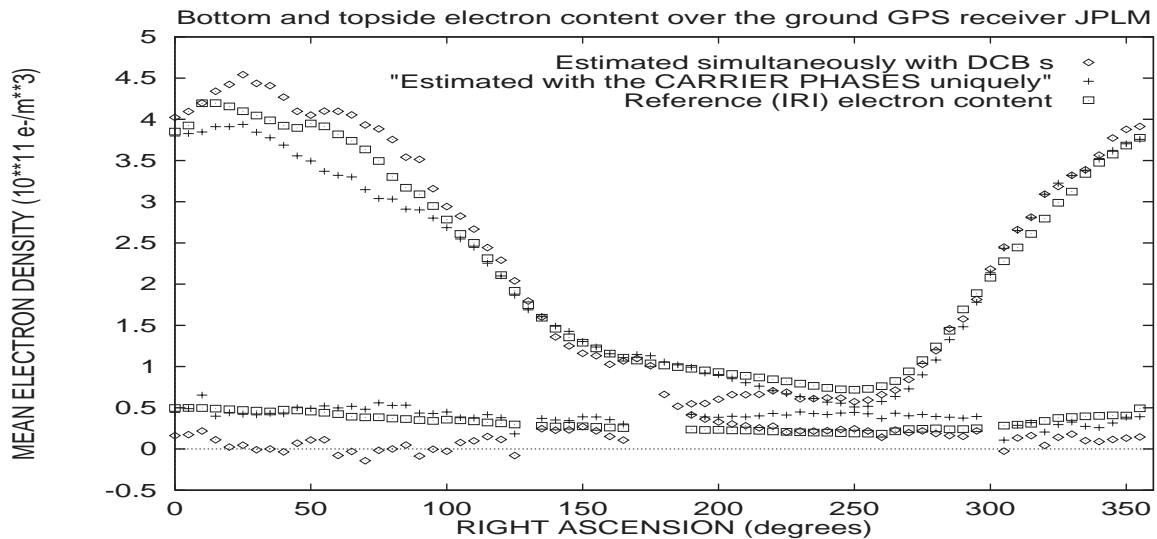


Fig. 1. Comparison, for the IGS station JPLM (6 April 1993), of the bottom and topside electron content estimation (two layer tomographic model) using differences of carrier phases (crosses) and estimating differential code biases — DCB — with code data (diamonds). The reference IRI values are represented by squares. The results are quite equivalent, in spite of the errors that would affect the DCB strategy being neglected in this synthetic dataset (see also Table 1).

Table 1  
Total electron content (TEC) carrier phase differences Eq. (1) vs delay code biases approach Eq. (2)<sup>a</sup>

Height (km)	$m_1$	$\sigma_1$	$rms_1$	$m_2$	$\sigma_2$	$rms_2$	$m_{IRI}$
	(10 <sup>11</sup> electrons/m <sup>3</sup> )						
TEC	0.02	0.23	0.23	-0.07	0.30	0.31	1.20
400	-0.10	0.03	0.03	0.06	0.34	0.34	2.41
1080	0.09	0.18	0.20	-0.15	0.25	0.29	0.44

<sup>a</sup> First layer (60–740 km) and second layer (740–1420 km) electron content obtained with carrier phase differences Eq. (1) and with simultaneous delay code bias estimation — neglecting the code noise — Eq. (2): the mean, standard deviation and RMS of the differences with the reference IRI values, and the mean IRI value (last column) are shown in units of mean density. The semi-synthetic data set corresponds to the GPS geometry and IRI electron density values for IGS GPS receiver JPLM on 6 April 1993.

phases only can be affected by the multipath, of the order of  $\approx 0.1$  TECU.

As a typical example of how both strategies compare, in the absence of the error sources commented upon before, we have generated a semi-synthetic data set using the IRI electron densities for the IGS station

JPLM (longitude of 242° and latitude of 34°, approximately). The results (Fig. 1) show that the two approaches are quite equivalent. Notice that in a real data scenario our strategy (that used carrier phase differences) is not affected by the code noise, or by the instrumental delay assumptions. This is not the case when we estimate the instrumental biases.

2.2. Tomography

The problem is the estimation of the electron density  $N_e(\vec{r}, t)$  in Eq. (2). To do this, the ionosphere is decomposed into cells where the electron density is assumed to be constant. The optimum size of these cells is related to the sensitivity of the data to the electron density distribution. So, with ground data, only a coarse vertical resolution is possible, but a much better horizontal resolution (i.e. for TEC) can be obtained. We can consider, for instance, a typical equatorial gradient — with low solar activity — of 2 TECU/degree in a solar fixed reference frame. The cells used in this work, with horizontal sizes of  $10 \times 5^\circ$  and  $5 \times 2.5^\circ$  in local time and latitude, represent unmodelled variations of  $\approx 5$  and  $\approx 3$  TECU relative to the mean value. Larger cells, as used by other authors (Rius et al., 1997) with

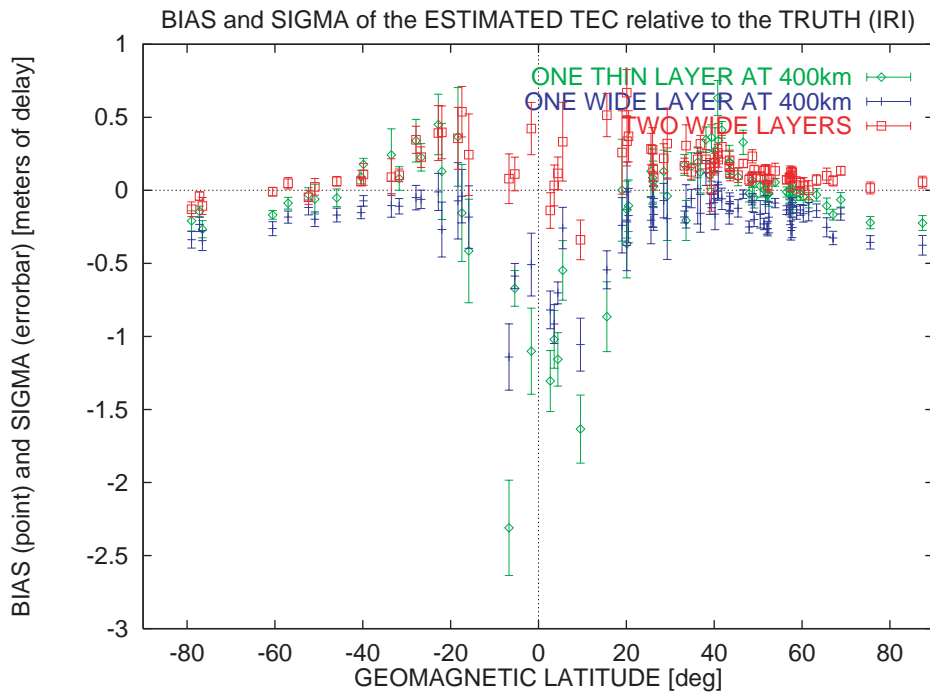


Fig. 2. The calibrations of the one thin layer GPS model (with boundaries at heights of 385 and 415 km, in green), the one wide layer model (boundaries at 60 and 740 km, in blue) and the two-layer model (boundaries at 60, 740 and 1420 km, in blue) are represented. The bias (points) and sigma (error bars) of the deviation between the estimated and the reference TEC (IRI) value are shown during the day on 1 June 1998, as a function of the geomagnetic latitude. The true geometry is used with ionospheric delays (synthetic observations) given by the IRI. Each point represents one single station in a set of 82 IGS selected stations.

cells of  $36 \times 18^\circ$  in horizontal size, must be avoided because they can present horizontal variations of 20 TECU relative to the mean value, and reach more than 50% of the TEC.

Then Eq. (2) for each arc of continuous carrier phases between a transmitter  $T$  and receiver  $R$  becomes:

$$\frac{\Delta \mathcal{L}_I}{\kappa} = \sum_i \sum_j \sum_k (N_e)_{i,j,k} [\Delta s_{i,j,k}^{t+\tau} - \Delta s_{i,j,k}^t] \quad (3)$$

where  $i, j, k$  are the indices for each cell corresponding to local time, geodetic latitude and height;  $(N_e)_{i,j,k}$  is the corresponding free electron density, and  $\Delta s_{i,j,k}^t$  is the length of the ray path crossing the “illuminated cells” at time  $t$ .

The values of the index  $k$  run over the different layers of the model (Table 1). Using only ground data two or three layers can be uniquely solved successfully (Juan et al., 1997). The use of two-layers allows a certain vertical structure, reducing the mismodelling due to a one-layer model, in particular avoiding the assumption of a fixed mapping function implicit with one thin layer. In this way the TEC estimation is improved: see top plot in Fig. 2 and caption, where a clear mismodelling appears in the range of  $\pm 20^\circ$  of geomagnetic latitude reaching  $-2$  m ( $\approx 50\%$  of the cor-

responding mean TEC value) for the one thin layer model (in green, with layer boundaries at 385 and 415 km in height) and reaching  $-1$  m ( $\approx 25\%$ ) for the one wide layer model (in blue, with layer boundaries at 60 and 680 km). The two layer model maintains the TEC mismodelling below 0.5 m ( $\approx 15\%$ ). On the other hand — not shown in the Figure — the two-layer model works quite well to get an unbiased TEC; the partial TEC estimations of the two-layer model present a correlated bias for geomagnetic latitudes between  $-30$  and  $30^\circ$ , where the density gradients are higher, reaching 25% for the first layer and 30–40% for the second layer.

The use of two layers can be understood as a model with a variable effective height driven by the data: this is especially adequate when the ionospheric gradient is large, i.e. close to solar maximum or close to the geomagnetic equator. Another advantage over the thin-layer models is that the tomographic models take into account an implicit horizontal gradient with one ray typically illuminating several cells. This is especially important in the low elevation rays, and again in the vicinity of the magnetic equator or close to solar maximum (see Fig. 3). Also, in this approach it is possible to impose continuity constraints locally between neighboring cells, providing in this manner the minimum information to invert Eq. (2) successfully.

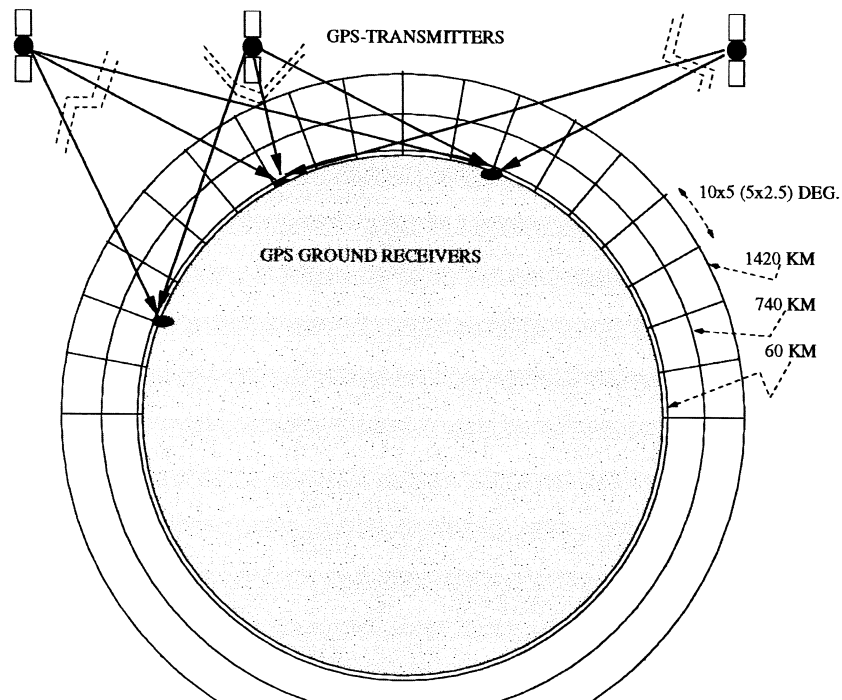


Fig. 3. Layout of the two-layer tomographic model adopted to estimate the electron content from IGS data.

Considering the above arguments, we have adopted a two-layer model for obtaining the total electron content from IGS data, with boundary heights 60–740–1420 km (see layout in Fig. 3).

2.3. Generating TEC maps

In order to have global TEC maps, two strategies can be used.

2.3.1. Station by station

Solving the TEC independently for each station,

obtaining the corresponding regional solution. The Kalman filtering (see, for instance, Hernández-Pajares et al., 1998a) is not necessary in this case, because each permanent receiver rotates continuously in the Sun fixed reference system that we consider and different cells are illuminated at different times. Another advantage of this approach is that we can estimate for each selected IGS station a regional electron content model, with high resolution ( $5 \times 2.5^\circ$  in local time and latitude, and 20 min in UT). These regional solutions can be combined — interpolated — and filling the spatial and temporal gaps later. This is the approach currently

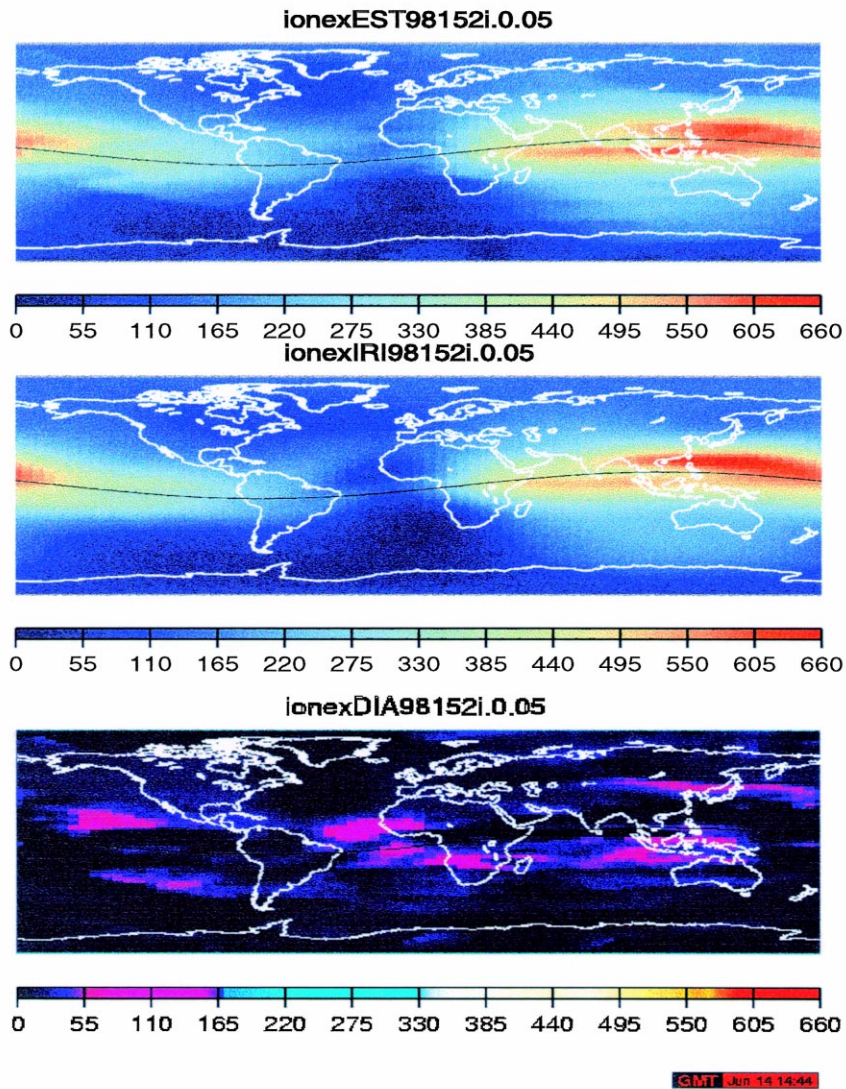


Fig. 4. Reconstruction of the IRI TEC (topside figure) from the IRI STEC's vs the reference IRI values (central plots) in units of 0.1 TECU on 1 June 1998 (03:00–05:00 UT). The difference is represented in the bottomsides plots (these figures have been produced with the software package GMT, of Wessel and Smith (1995)).

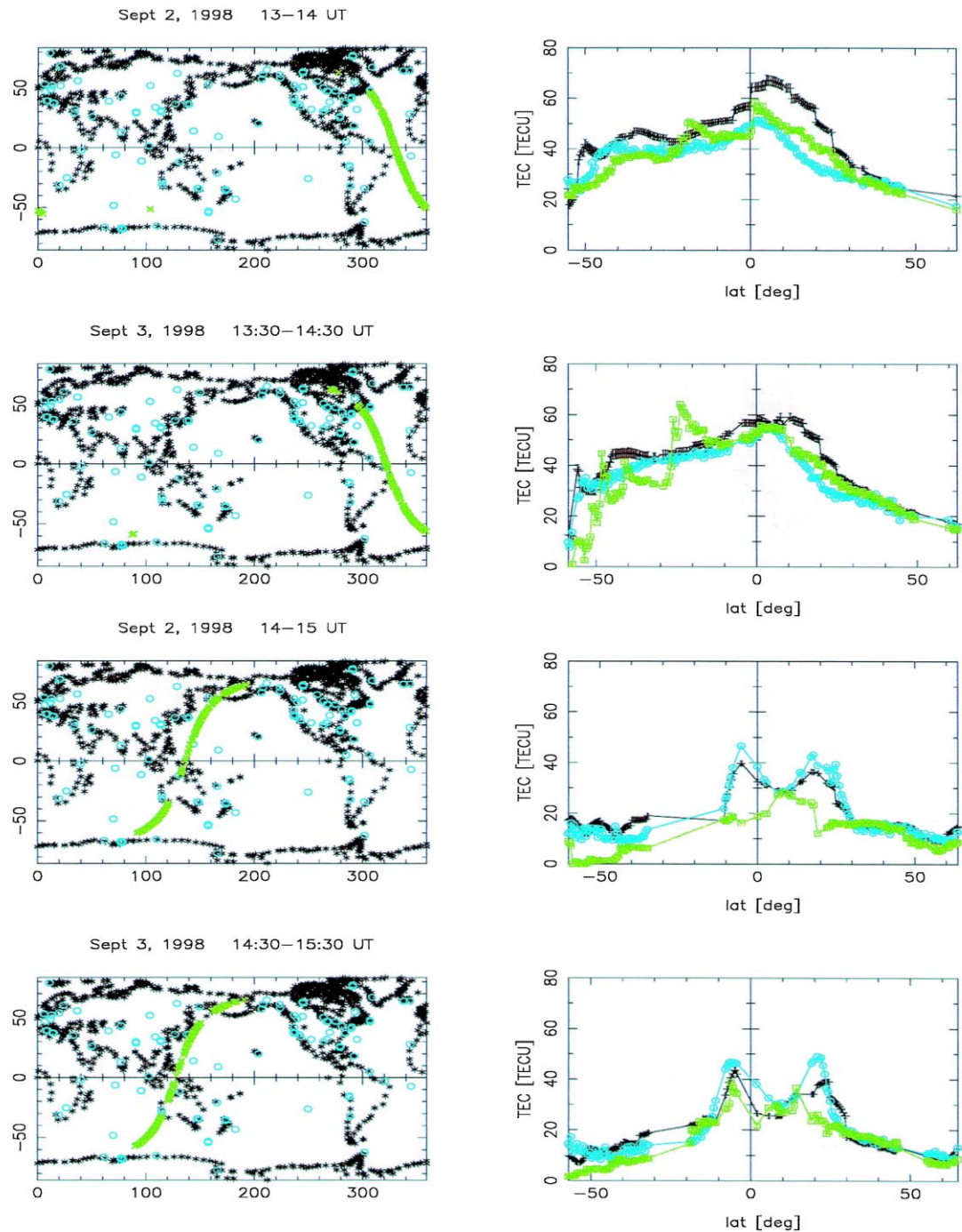


Fig. 5. In the plots of the second column the comparison of TOPEX TEC (blue line), GPS TEC multistation (black line) and station-by-station (green line) obtained by the authors are shown as a function of latitude. They correspond to a sample of equivalent TOPEX tracks (see corresponding map in column 1) for 2 and 3 September 1998. The IGS stations considered are marked with circles.

adopted in the daily UPC ionospheric product generation.

2.3.2. Multistation

Where the data coming from all the selected IGS receivers are considered simultaneously in a global tomographic model, and the electron content estimate is updated with the Kalman filtering scheme. In this

way, most of the interpolation is implicit in this approach. In order to have a global solution for each batch we have to use a lower resolution of  $10 \times 5^\circ$  in local time and latitude, and 2 h in UT (the batch update period).

The sparseness of the IGS permanent GPS receivers, especially outside North America and Europe, produce important gaps in space and time in the tomographic

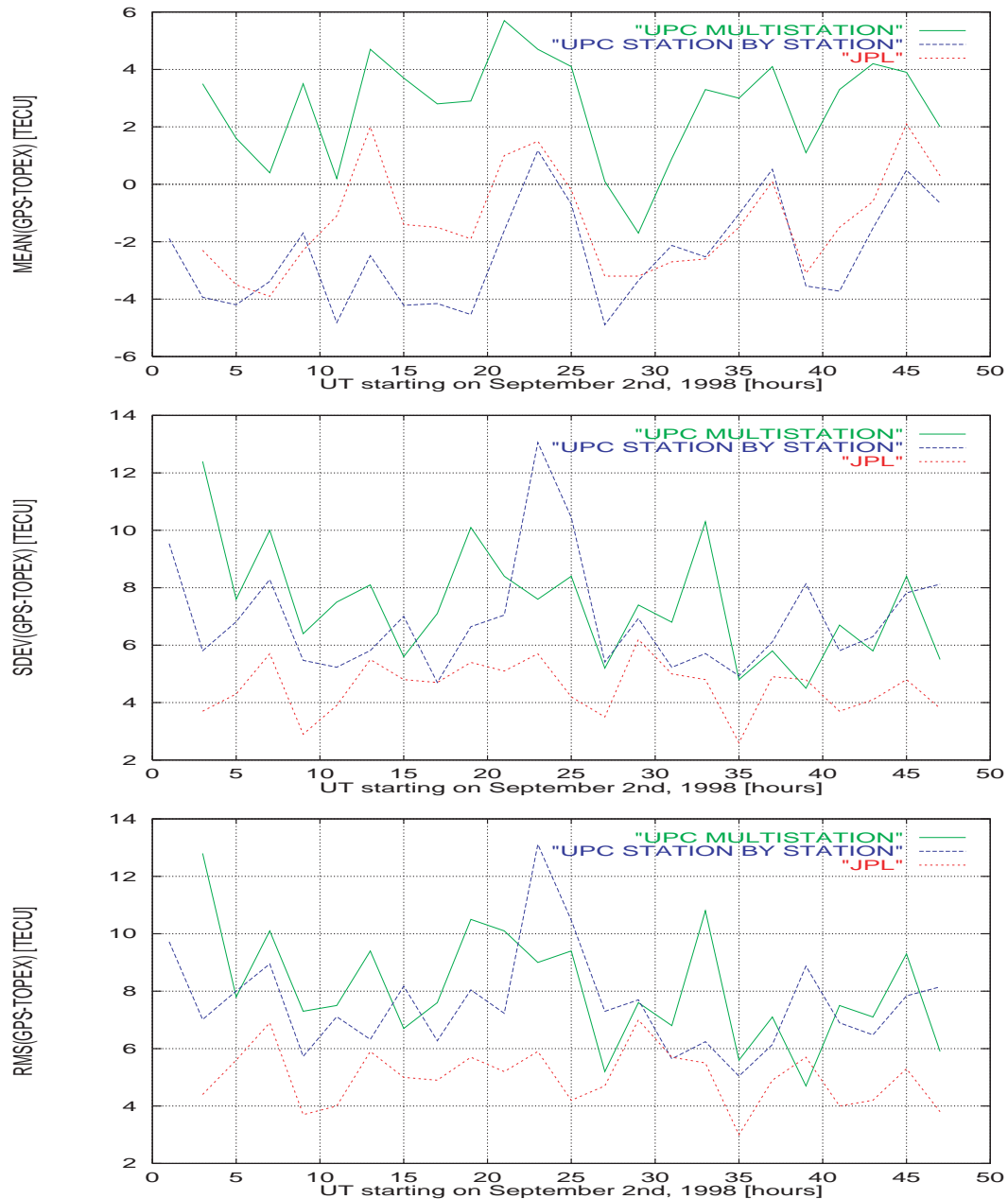


Fig. 6. Mean, standard deviation and RMS (in TECU) of the UPC (multistation and station-by-station approach) and JPL TEC differences from the TOPEX TEC each 2 h, for all the available TOPEX tracks of 2 and 3 September 1998.

model, due to the lack of data. In the multistation approach many of these gaps are filled by the Kalman filter algorithm, but in the station-by-station strategy it is necessary to interpolate the regional solutions in order to have the global TEC maps. In this case the interpolation is done using the typical stationarity on a solar fixed reference frame because, in the absence of ionospheric storms but in extreme conditions, the TEC temporal variation in a given cell is less than 5% of the mean value.

For the interpolation, the Gaussian radial basis function approach is used (Haykin, 1994, 269–274). It consists of a weighted mean of the station-by-station TEC estimates. The weights are Gaussian functions of the distance in local time, latitude and UT of the TEC direct estimates to the point where the interpolated value is desired. The scale parameters  $\sigma$ , or correlation radii, have been chosen equal to the pixel size (5 and 2.5° in local time and latitude, and 2 h in UT), in such a way that the smoothing is minimal. Notice that we do not use any climatological model or strong smoothing to fill the gaps of estimates in local time, latitude and UT. Thus, the information comes from the closest estimates in space and time, and on the stationarity assumption in the solar fixed reference frame.

### 3. Calibration with the IRI

To characterize the implicit error in the estimation of the electron content, we have also generated a semi-synthetic dataset with the real ray geometry and using the electron densities provided by the climatological ionospheric model IRI to compute the  $\mathcal{L}_1$  carrier phase observations. Taking into account that the electron content is estimated only with the carrier phases, whose observational error is negligible in this problem ( $\leq 1$  cm), it is reasonable to think that the mismodelling obtained should be similar to that obtained with the real dataset. Once the inverse problem is solved using the station-by-station strategy, the results are compared with the IRI corresponding vertical electron contents.

The comparison for half a solar cycle, for the regional solutions of two typical equatorial and midlatitude IGS stations (Bilitza et al., 1998, Fig. 3) provides equivalent results to those summarized in Fig. 2 for a large set of stations at different geomagnetic latitudes. Both studies show a mismodelling of the two-layer model typically below 5 TECU for high TEC values with a standard deviation of few TECU; the topside and bottomside electron contents can show a correlated pattern that basically does not affect the TEC estimation.

In Fig. 4 the estimated and IRI reference TEC, and its difference, are plotted for a global ionospheric map,

corresponding to a typical batch of 2 h (04:00–06:00 UT, on 1 June 1998). In the comparison the effect of the lack of data over the oceans can be clearly seen. The discrepancies can reach more than 10 TECU in these non-illuminated areas. The full comparison can be found in Hernández-Pajares et al. (1998b).

It is clear, also in the simulated scenario with low temporal variation, that the results are worst in the regions with few (if any) data, where the interpolation drives the final computation. These effects can also be observed when the multistation approach is used.

### 4. Comparison with TOPEX altimetric data

Despite the fact that a bias of few TECU seems to affect the TOPEX Poseidon data, the direct estimation of the TOPEX TEC over the oceans provides a good opportunity to compare with results obtained by GPS. These estimations rely mainly on the interpolation scheme because over the oceans few GPS data are available.

As an example, in Fig. 5 it can be seen that the GPS TEC estimation with both multistation and single station strategies are compatible with the TOPEX TEC, mainly when enough data are available. A peak can be seen in the multistation strategy, on 3 September, 13:30–14:30 UT. It is a good example of the effect of an important lack of data and then direct GPS estimates over this part of the TOPEX track, combined with the simple interpolation scheme — radial basis function — that avoids the use of any a-priori model.

The overall comparison for 2 and 3 September 1998 (53 TOPEX passes and 7700 individual TOPEX observations, 80 GPS stations and more than 1,000,000 individual GPS observations) is summarized in Fig. 6. It shows the mean, standard deviation and RMS of the results with multistation and station-by-station strategies presented by the authors (UPC) relative to TOPEX plotted each 2 h for both days. The corresponding estimates obtained by JPL/CALTECH are also presented.

The bias with the multistation strategy is typically positive, with values around 2–3 TECU. This result, in spite of the uncertainty of a few TECU with the TOPEX bias, could be compatible with the plasmaspheric component included in the TEC computed with GPS. The peak in Fig. 6 at 23:00 UT on 2 September 1998 is due to the lack of GPS data over the oceans that specially affects to the station-by-station solution; that starts a new and independent solution each day for each station, because it does not implement the Kalman filter.

The practical conclusion is that both approaches (multistation and station-by-station) provides results of

similar quality (with similar RMS relative to TOPEX of 7–8 TECU), but the multistation approach is a bit more stable, specially in those parts with a lack of data because the spatial and temporal interpolation is done simultaneously in the Kalman filter.

### 5. Another scenario: combining ionosonde and GPS data

We have seen that the horizontal structure of the ionospheric electron content (i.e. TEC) can be computed using a tomographic model with coarse vertical description, i.e. with topside and bottomside electron contents. To improve the vertical resolution it is necessary to use data, with complementary geometry, that can be gathered from Low Earth Orbiter (LEO) GPS receivers (Hernández-Pajares et al., 1998a). Another possibility is to use direct electron density estimations provided, for instance, by ionosondes combined with GPS data. The ionosondes provide direct estimations of the vertical electron density profile up to the  $f_0F_2$  maximum. Then, both observational sys-

tems can be combined, taking into account that they complement each other well in:

- Horizontal resolution, mainly contained in the ground GPS data, and in the large number of permanent IGS stations,
- Vertical resolution, very high up to the  $f_0F_2$  maximum in the ionosonde data, and with topside information from ground GPS data.

#### 5.1. Data set

In the same way as in the calibration with GPS ground data, and using the geometry of the real dataset for 2 November 1997, two semi-synthetic data sets have been generated, taking density values provided by the IRI, one for low solar activity (November 1997) and another for medium solar activity (November 1998). The GPS receivers are shown in Fig. 7. The ionosonde is very close to EBRE, at 0 degrees in longitude and 40 degrees in latitude, approximately. The results obtained with the 1997 and 1998 datasets are

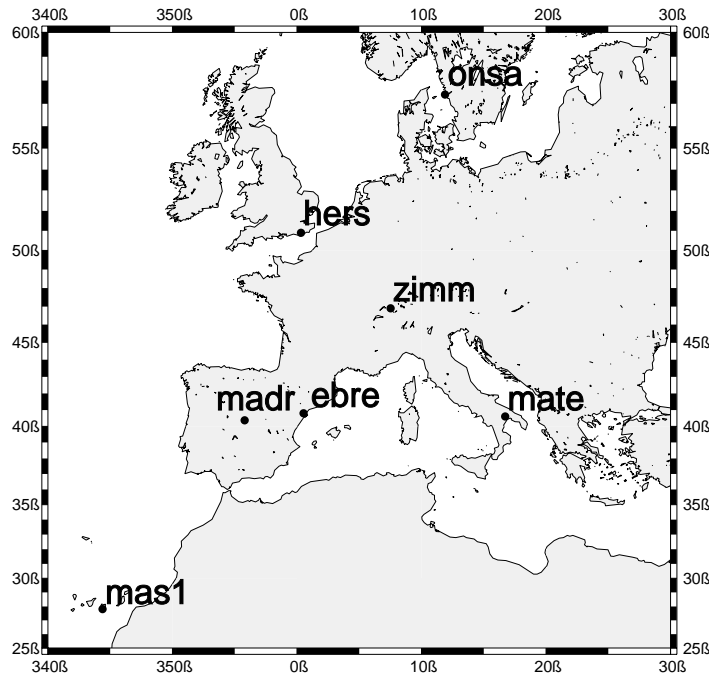


Fig. 7. GPS receivers for which dual frequency data are combined with the ionosonde data to recover the electron content distribution.

similar, so we show those corresponding to November 1997, when real ionosonde and GPS data were available.

### 5.2. Tomographic model

The tomographic model consists of a grid of  $36 \times 20 \times 5$  cells in local time, latitude and height, centred approximately on noon and between 15 and 70° in latitude, in correspondence with Fig. 7. The resolution is  $5 \times 3^\circ$  in local time and latitude (the reference system is Sun fixed) and with five layers defined with boundary heights at 75–125–175–250–650–2000 km. Kalman filtering is not necessary because cells with different local times are illuminated at different epochs due to the Earth's rotation and to the proximity of the stations in longitude.

### 5.3. Results

The effect of a combined use of ionosonde and GPS data can be seen in Fig. 8: the estimation of mean densities are clearly improved when GPS and ionosonde data are used, allowing the extension of the electron content vertical structure above the maximum height reached with the ionosonde.

Table 2 shows a negligible bias in the mean electron density estimation when ionosonde data are combined with the GPS dataset. However, this situation is quite different when only GPS data are used, with important mismodelling in form of transference between layers.

## 6. Conclusions

The main topics of this paper are:

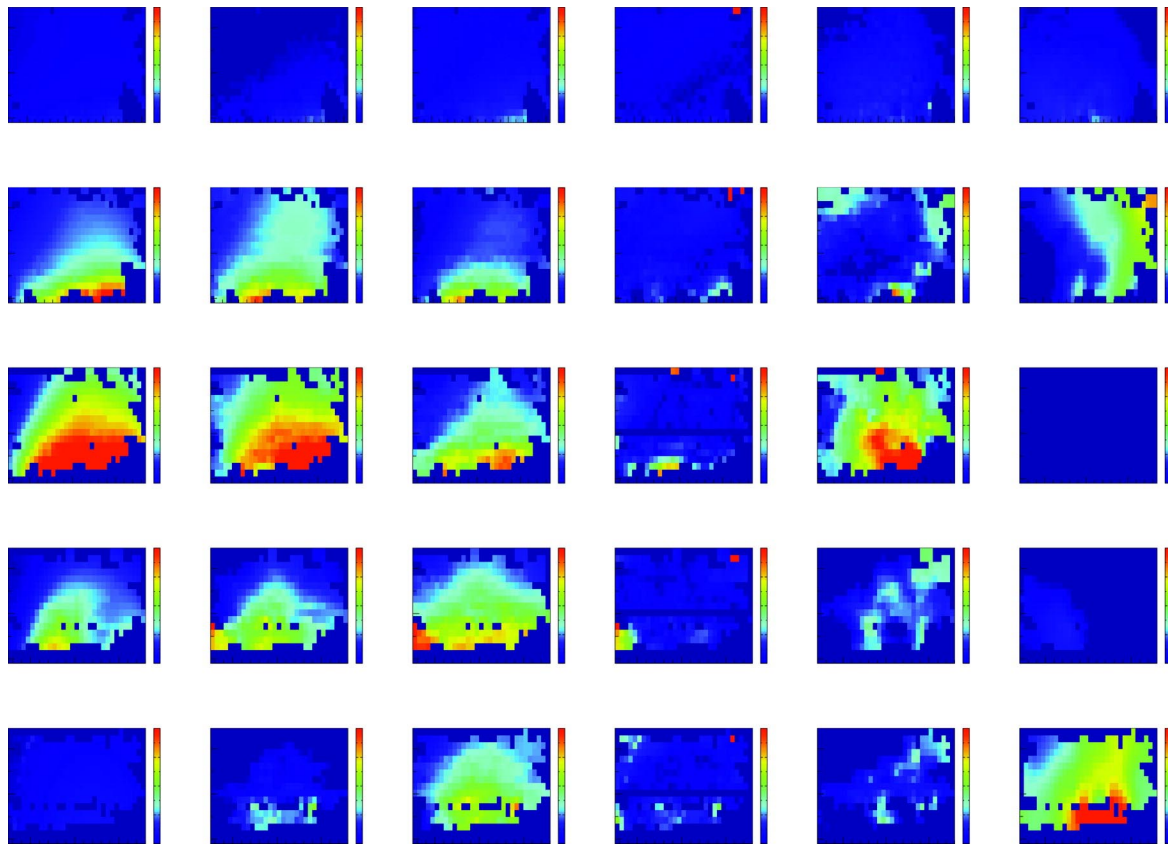


Fig. 8. Each plot represents the corresponding mean electron density for layer 1 (bottom) to layer 5 (top), for the cases of reference IRI distribution (column 1), estimated with semi-synthetic GPS and ionosonde data (column 2), only semi-synthetic GPS data (column 3), the absolute value of its difference column 2–column 1 (column 4), the estimation with real ground GPS and ionosonde data (column 5), and the estimation with only real GPS ground data (column 6). The colour scale ranges from 0 (black) to  $8 \times 10^{11}$  electrons/m<sup>3</sup> (red), the axes run between 15 and 70° in latitude and between 125 and 300° in right ascension, i.e. from 5.8 to 17.7 h in Local Time approximately (the Sun is at 217° of right ascension and at  $-15^\circ$  of declination). The geometry and values of the semi-synthetic data set corresponds to 2 November 1997.

Table 2

Summary of the results of the combination of ground semi-synthetic GPS and ionosonde data for the low solar activity dataset (2 November 1997)<sup>a</sup>

Layer	Height (km)	$m_1$	$\sigma_1$	$rms_1$	$m_2$	$\sigma_2$	$rms_2$	$m_{IRI}$
		$(10^{11} \text{ e}^-/\text{m}^3)$						
1	75–125	−0.2	1.1	1.1	2.3	1.9	3.0	0.4
2	125–175	0.3	2.7	2.7	1.4	3.4	3.7	1.9
3	175–250	−0.3	5.3	5.3	−2.4	2.0	3.1	5.1
4	250–650	0.4	2.9	2.9	−0.6	1.9	2.0	2.2
5	650–2000	−0.1	0.5	0.5	0.3	0.7	0.7	0.3

<sup>a</sup> The layer number, boundary heights, and the mean  $m_j$ , standard deviation  $\sigma_j$  and RMS  $rms_j$  of the differences of the estimated electron density with ground GPS and ionosonde data relative to the IRI values ( $j = 1$ ) and the difference only with ground GPS data ( $j = 2$ ) are shown. Also the mean reference (IRI) value is included in the last column (all these are given in  $10^{11} \text{ e}^-/\text{m}^3$ ).

- The use of new strategies for the TEC estimation: a two-layer tomographic model improves the results compared with the one-layer model, particularly when there are large TEC gradients. The feasibility of using only carrier phase data to compute the TEC, without aligning with the pseudo-range and without estimating the delay code biases as is done classically, has also been shown.
- The generation of global TEC maps: the retrieval of TEC from synthetic data in a regional solution (driven by GPS data only) is quite satisfactory, at the level of 5 TECU or better. In the generation of global TEC maps, the retrieval of synthetic TEC data is worst ( $\approx 10$  TECU) in areas where few GPS data are available. Using real data, the comparison with the TOPEX TEC, mainly measured over the oceans far from the IGS stations, are compatible with the errors commented upon before.
- The combination of ionosonde and ground GPS data allows the extension of the high resolution electron density bottomside profile given by the ionosonde to more than 20 degrees to the North and South. This is possible thanks to the ground GPS data that allow such an extrapolation due to the small but existing vertical information contained in the low elevation GPS ground observations.

## Acknowledgements

We thank the IGS community for providing the ground receiver data and the Ebre Observatory (Roquetes, Spain) for the ionosonde data. We are grateful to D. Bilitza for providing the IRI model, and to JPL/CALTECH for providing TOPEX and JPL estimates to perform the corresponding comparison. This work has been partially supported by the Spanish CICYT project TIC97-0993-C02-01.

## References

- Bilitza, D., 1990. International Reference Ionosphere 1990. URSI/COSPAR, NSSDC/WDC-A-R&S 90–22.
- Bilitza, D., Hernández-Pajares, M., Juan, J.M., Sanz, J., 1998. Comparison between IRI and GPS-IGS derived electron content during 1991–97. *Physics and Chemistry of the Earth* 24 (4), 311–319.
- Feltens, J., Schaer, S., 1998. IGS products for the ionosphere. In: *Proceedings of the IGS Analysis Center Workshop*, ESA/ESOC Darmstadt, Germany, pp. 225–232.
- Haykin, S., 1994. *Neural Networks: A Comprehensive Foundation*. Macmillan, New York.
- Hernández-Pajares, M., Juan, J.M., Sanz, J., Solé, J.G., 1998a. Global observation of the ionospheric electronic response to solar events using ground and LEO GPS data. *Journal of Geophysical Research* 103 (A9), 20789–20796.
- Hernández-Pajares, M., Juan, J.M., Sanz, J., 1998b. Calibration of the gAGE/UPC daily ionospheric product using IGS GPS data (gAGE-dip). [http://maite152.upc.es/ionex/GPS\\_calibration/GPS](http://maite152.upc.es/ionex/GPS_calibration/GPS).
- Juan, J.M., Rius, A., Hernández-Pajares, M., Sanz, J., 1997. A two-layer model of the ionosphere using global positioning system data. *Geophysical Research Letters* 24, 393–396.
- Mannucci, A.J., Wilson, B.D., Yuan, D.N., Ho, C.H., Lindqwister, U.J., Runge, T.F., 1998. A global mapping technique for GPS-derived ionospheric total electron content measurements. *Radio Science* 33, 565–582.
- Rius, A., Ruffini, G., Cucurull, L., 1997. Improving the resolution of ionospheric tomography with GPS occultations. *Geophysical Research Letters* 24, 2291–2295.
- Wessel, P., Smith, W.H.F., 1995. New version of the generic mapping tools released. *EOS Transactions AGU* 76, 326.